Passive Euro-American Terahertz Camera (PEAT-CAM): Passive indoors THz imaging at video rates for security applications

Arttu Luukanen*[a], Leif Grönberg[b], Panu Helistö[b], Jari. S. Penttilä[b], Heikki Seppä[b], Hannu Sipola[b], Charles R. Dietlein[c,d], and Erich N. Grossman[c]

[a] Millimetre-wave Laboratory of Finland – MilliLab, Tietotie 3, 02044 Espoo, Finland

[b]VTT Technical Research Center of Finland, Tietotie 3, 02044 Espoo, Finland

[c§]Optoelectronics Division, National Institute of Standards and Technology, Boulder, CO

[d§]Electrical and Computer Engineering Dept., Univ. of Colorado, Boulder, CO

ABSTRACT

The objective of this program is to demonstrate a system capable of passive indoors detection and *identification* of concealed threat items hidden underneath the clothing of non-cooperative subjects from a stand-off distance of several meters. To meet this difficult task, we are constructing an imaging system utilising superconducting ultrawideband antenna-coupled microbolometers, coupled to innovative room temperature read-out electronics, and operated within a cryogen-free pulse tube refrigerator. Previously, we have demonstrated that these devices are capable of a Noise Equivalent Temperature Difference (NETD) of 125 mK over a pre-detection bandwidth from 0.2-1 THz using a post-detection integration time of 30 ms. Further improvements on our devices are reducing this number to a few tens of mK. Such an exquisite sensitivity is necessary in order to achieve the undoubtedly stringent requirements for low false positive alarm rate combined with high probability of detection dictated by the application. Our technological approach allows for excellent per frame NETD (objective 0.5 K or below at 30 Hz frame rate), and is also amenable to multispectral (colour) imagery that enhances the discrimination of innocuous objects against real threats. In the paper we present results obtained with an 8-pixel subarray from our linear array of 128 pixels constructed using a modular approach. Two-dimensional imaging will be achieved by the use of conical scanning.

Keywords: Bolometer, concealed weapons, imaging, millimeter-wave, terahertz, ultrabroadband

1. INTRODUCTION

While there has been tremendous development of passive mm-wave and THz imaging systems over the last several years, it is evident from published data that the passive systems, while powerful anomaly detectors by their virtues, have limited performance in conditions where illumination is not used. In our previous work [1], we have argued that the radiometric (thermal) resolution for a passive imager needs to be better than about 0.5 K/pixel/frame in order to carry out reliable detection and identification in uncontrolled indoors environment. Active systems can achieve impressive performance, but do need either a flood illumination of the scene, or are faced with the artifacts caused by directional illumination in the case of true stand-off detection. Also, the limited output power of THz sources limit the operation of stand-off systems to relatively close range.

The primary objective of the PEAT-CAM program is to design, construct and demonstrate a real-time, passive ultrawideband THz imager for homeland security applications with a NETD better than 0.5 K (30 ms per-pixel integration time). This program is a natural continuation of our previous work [2,3,4], in which we demonstrated single-pixel scanned imagery with a superconducting bolometer of the same type. However, this demonstration was carried out within a liquid Helium dewar, clearly ruling out any extensive field tests or operation for extended periods of time outside of the laboratory. Thus, our present program has a heavy emphasis on transferring the technology to operate within a cryogen-free pulse-tube refrigerator. Such cryocoolers are commercially available, can operate continuously without requiring operator attention for several years, and are simple to operate. From the system standpoint however,

§ Contribution of the U.S. Government, not subject to copyright within the U.S.

* email: arttu.luukanen@vtt.fi

Passive Millimeter-Wave Imaging Technology X, edited by Roger Appleby, David A. Wikner,
Proc. of SPIE Vol. 6548, 654808, (2007) · 0277-786X/07/$18 · doi: 10.1117/12.719778

the cryocooler environment poses substantial challenges with respect to dealing with the EMI environment, as well as mechanical and thermal oscillations.

It should be noted that the detector technology can be readily modified for "colour" imaging in the THz using either tuneable band-pass filter [5], or by the use of several overlapping frequency channels. This paper is a brief summary of the overall system design, and will not discuss in detail the scanning imaging optics of the system, which will be discussed in detail in subsequent publications.

2. DETECTOR CHARACTERISTICS

2.1 Principle of operation

As the detector, we employ a variation of the antenna-coupled microbolometer [1,6-8]. The operating principle of bolometric detectors is based on a variation in temperature of a thermally isolated termination of the antenna, caused by variations in the incident RF power. By sensitive thermometry, the variations in the incident power can be determined. The detector consists of a self-similar logarithmic spiral antenna, coupled to a suspended strip of superconductor (NbN in the detectors fabricated at VTT, Nb for detectors fabricated by NIST). The nominal RF bandwidth of the antenna is 0.2 to 1.8, 3.6 or 5.4 THz, depending on the antenna feed dimensions. In our case, the NbN strip acts both as the resistive termination for the antenna, as well as the thermometer: when cooled to below its superconducting critical temperature T_c, a constant voltage bias placed across the bridge results to phase separation, where the centremost part of the bridge remains in normal state (resistive), while the ends remain superconducting. RF power is dissipated mostly within the normal state region, and variations in the RF power affect the size of the normal state region of the bridge. The corresponding modulation in the current is the (baseband) signal.

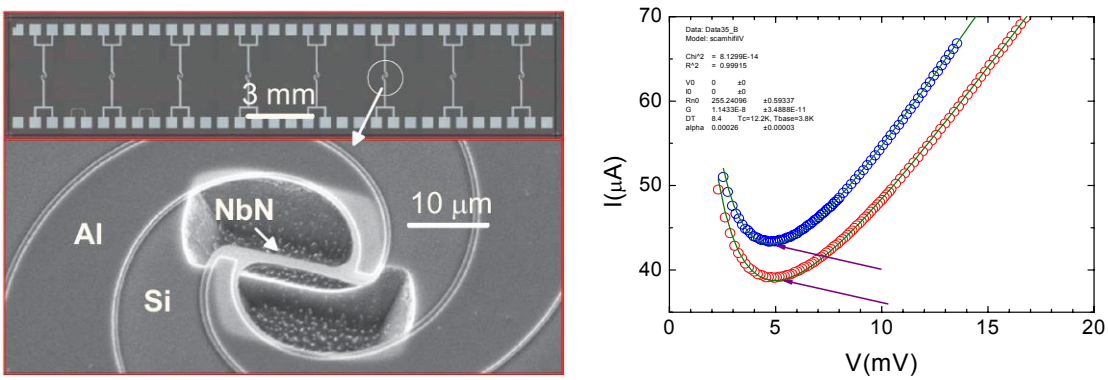

Fig 1. (Left) A scanning electron micrograph of a 8 x 1 pixel sub-array (top of figure), under which a close up of the feed region of the antenna is shown. (Right) The current-voltage characteristics of two NbN detectors, measured simultaneously within a standard PT cryocooler. The optimum operation point is indicated by the arrows.

The theoretical modeling of the bridge is very simple, and has been reported elsewhere [2,4-6]. In short, the DC current-voltage characteristics have the simple form $I=V/R_N+V_0^2/V$, where R_N is the resistance of the entire bridge in the normal state, $V_0=(G_{th}\Delta T R_N)^{1/2}$, G_{th} is the thermal conductance between the bridge and the substrate, and $\Delta T=Tc-T_0$ is the temperature difference between the bolometer and the heat sink (at temperature T_0). The voltage V_0 also corresponds to the voltage at the minimum of the current in the I-V curve (see Fig. 1). As will be explained below, the optimum operating point for the system is close to V_0.

The electrical and optical characterization of both Nb and NbN devices has been recently carried out, and is reported in [9]. From the measured I-V curves, we can extract a fitted value for the important parameter G_{th}. For our NbN devices, the value for G_{th} is typically about 10 nW/K, corresponding to an phonon noise limited electrical noise equivalent power NEP of $9\cdot10^{-15}$ W/Hz$^{1/2}$.

2.2 Array configuration

The 128 x 1 pixel array will be constructed out of 8x1 pixel sub-arrays, or "modules", each of which are attached to a copper cold finger (see Fig. 2). Each antenna is coupled to the incident optical beam through a 2 mm diameter hemispherical Si substrate lens (thickness 0.78 mm). A detector to detector spacing of 3 mm was chosen as a compromise between attainable instantaneous field of view and the physical array size, resulting to a length of 40 cm for the entire array. Each module is connected at 4 K to a pcb interface board, which houses the connectors for cryogenic flexible cabling that carries out the signals to the room temperature preamplifiers.

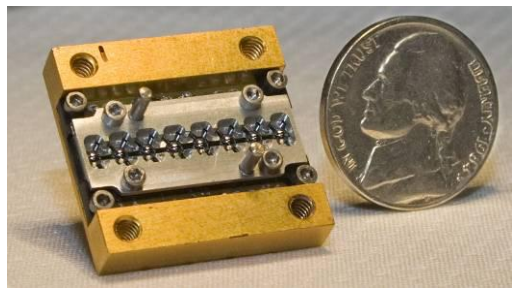

3. NbN DETECTOR FABRICATION

The superconducting bolometers are fabricated using standard photolithographic process on a 100 mm diameter Si wafer. The 495 μm thick substrate is of high resistivity Si (6 kΩcm < ρ < 16 kΩcm). Fabrication is carried out at the VTT microfabrication facility, and the details of the fabrication have been reported elsewhere [10]. The end result is a suspended NbN bolometer, as shown in Fig 3. Various bolometer designs have been fabricated. Typically, the NbN bolometer bridge dimensions are 8 μm x 2 μm, with a nominal thickness of 350 nm. Depending on the exact sputtering conditions, these dimensions typically yield devices with a square resistance of about 30 Ω. On the wafer, there are two types of chips: 5 mm x 5 mm chips with three devices on each for single pixel applications, as well as 8x1 pixel linear arrays for our passive 128 pixel camera. The array chips are distributed across the center of the wafer (see Fig. 3). The overall yield of the process was 69 % in terms of device square resistance (R□); However, the yield on the 8x1 pixel arrays was 100 %, with a standard deviation less than 10 % in R□. The spread in R□ is consistent with the radial location of the device from the wafer center point due to the uneven etch rate of NbN across the wafer.

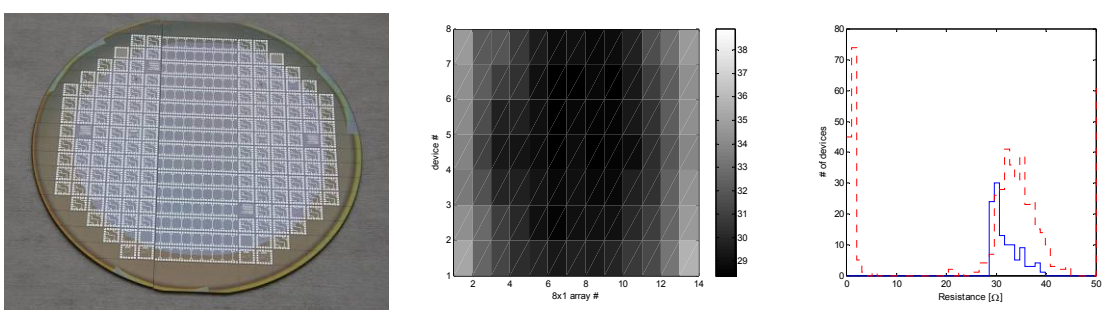

Fig 3. (Left) A photograph of the detector wafer after processing and prior to the device dice-up. (Middle) Map of the sheet resistance of the 8x1 pixel array bolometers. (Right) Histograms of the sheet resistance across the wafer. Solid line corresponds to the 8x1 pixel modules, while the dashed line represents the distribution of the sheet resistances for the 5x5 mm2 chips

4. READOUT ELECTRONICS

Noise in our bolometers consists of three main components: noise due to fluctuations of energy between the thermally isolated bridge and the heat sink (substrate), electrical noise (i.e. Johnson noise), and noise from the amplifier. The first two are intrinsic to the bolometer, and roughly comparable in magnitude close to V_0. Principle of the readout is shown in Fig. 4. Its operation is described in detail in [11]. A low noise room temperature amplifier reads out the voltage over the

bolometer and via electrical feedback maintains it constant. In addition to electrical feedback, electro-thermal feedback (ETF) is utilized to drive the bolometer near V_0, making the dynamic impedance $Z_d = dV/dI$ diverge at low frequencies. In this way, the voltage noise of the amplifier becomes insignificant compared to the bolometer noise. Current noise of a JFET input is made easily lower than the noise of a 4 K bolometer.

For the 128 x 1 pixel array, we employ a brute-force scale-up of the single channel electronics. The array readout electronics consists of preamplifier "cards" with 8 channels on each card. Each one of the cards connects to a "motherboard" via a PCI connector. A custom built low noise power supply powers the entire readout electronics box.

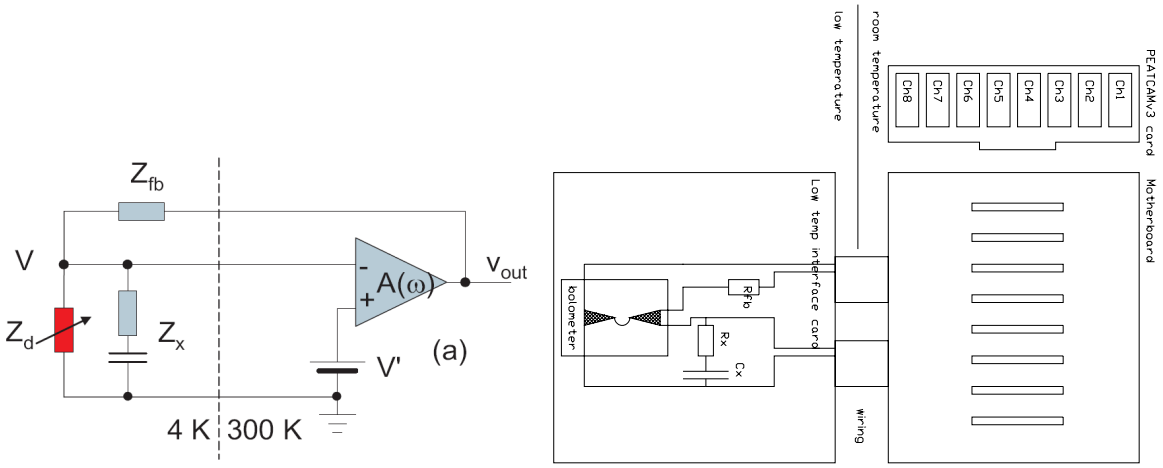

Fig.4 (Left) The basic operating schematic of the thermo-electrical readout. (Right) An overview of the electronics architecture.

One of the challenges with the multiplication of the electronics is the interfacing between the readout and the bolometer. To do this, we have designed and fabricated custom cryogenic flexible cabling, which facilitates easy connections to all bolometers, while the amount of parasitic heat carried to the cryogenic stages is minimized.

While we have demonstrated the noise matching of the detector to the readout electronics successfully, the architecture does currently suffer from excessive amounts of electromagnetic pickup. While differential readout architecture can remove most of the common-mode pickup induced to the wiring between the preamplifier and the bolometer, it does not completely remove the EMI issue. This is because interference currents induced in the wiring are in fact *detected* by the bolometer (which is basically sensitive to any power from DC to THz). Efforts are underway in minimizing EMI detection.

5. CRYOGENIC SUBSYSTEM

The transfer of operation from a liquid Helium dewar to a cryogen free system is one of the foci of our current effort. This seemingly straightforward task is complicated by the vastly different EMI, mechanical vibration, and thermal oscillation environment of the cryocooler, in addition to the sheer size of the cryogenic detector array. Commercially available cryocoolers are available from several manufacturers. The coolers are typically based on either the Gifford-McMahon or the so-called Pulse-Tube heat cycles. We have chosen to use a pulse-tube cryocooler, which has the attractive feature that there are no moving parts in the cryogenic part of the refrigerator. This facilitates care free operation up to ~20 000 hours. After that, a sorption filter change is needed, but this is a simple operation that can be carried out by a non-specialist on-site. At VTT, a dual-stage Cryomech PT403 pulse-tube cold head was chosen, which provides at least 230 mW and 9 W of cooling power at the 2nd (at ~4 K) and 1st (at ~65 K) stages, respectively [12]. These numbers are obtained when the cold-head is combined with the Cryomech CP830 compressor. The (water cooled) compressor unit (measuring 46 cm x 46 cm x 56 cm) consumes 3.3 kW of electrical power, and can be run of a single phase mains line.

To minimize the effect of mechanical vibrations, we have designed the cryocooler to be mechanically decoupled from the cold finger which supports the detector array. Structural support is provided by custom designed low thermal conductivity posts which support the vibration-free 65 K and 4 K stages and radiation shields from the top flange of the

vacuum can. The thermal couplings between the PT "insert" and the corresponding stages of the unit are made with flexible heat links. The total radiative & conductive heat loads to the 2nd and 1st stages of the PT cooler are estimated to be ~60 mW and ~8 W, respectively. The radiative burden has been calculated assuming 10 % enclosures' emissivity which is likely overly pessimistic for the highly polished radiation shields. With this amount of heat loading on the stages, the 1st and 2nd stages of the cooler are expected to reach base temperatures of ~3.5 K and ~60 K, respectively.

The optical coupling between the detector array and the conical scanning optics is carried out through a window 51 cm in length and 3 cm in width, located at the bottom of the vacuum can. The vacuum window material is 4 mm thick sheet of high density polyethlylene (HDPE), which provides good transmission throughout the entire detector bandwidth. Between the HDPE window and the detector array, there are Zitex [13] scattering low-pass filters at the 1st and 2nd stages of the cryostat for infrared blockage. The Zitex type G110 has been characterized in the past [14], and has excellent in-band transmission characteristics (~90 % for single sheets) and a 3 dB high frequency cut-off at about 4.3 THz. This bandwidth is in fact somewhat in excess of what is desirable for the imaging applications as atmospheric as well as clothing transmittance becomes very poor at frequencies well beyond 1 THz.

At this stage, two identical cryogenic systems have been constructed, of which the first one has been proven vacuum tight. Cooling trials are expected to commence in the near future. Finally, it should be noted that this 1st generation array refrigerator has been designed using very conservative design rules, leaving room for significant reduction in size and weight, as well as possibly reduction in the cooling power requirements for the pulse tube.

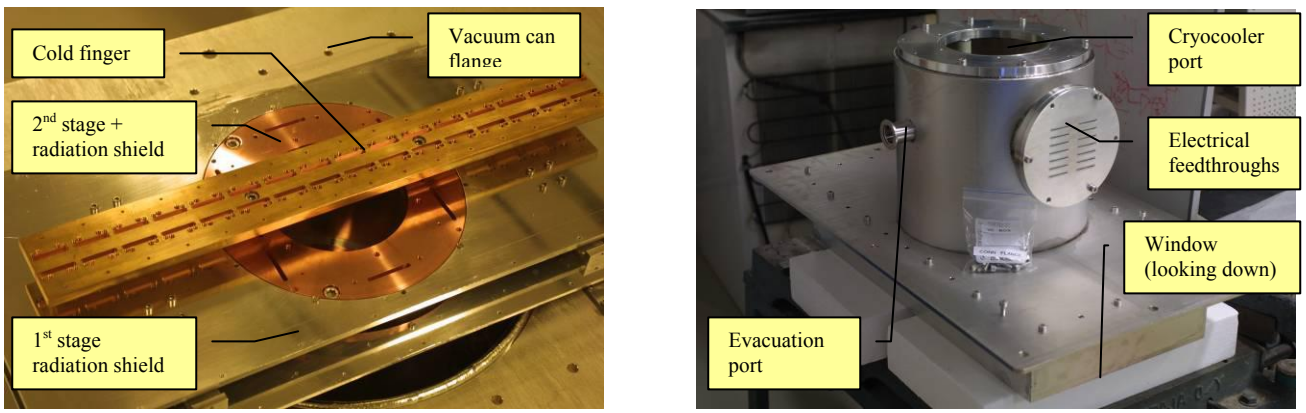

Fig. 5. (Left) The bottom of the cryostat with the bottom of the vacuum can removed, showing the linear cold finger onto which the 8x1 pixel sub-arrays will be mounted. (Right) Overview of the vacuum can, now right side up.

6. INITIAL TESTING WITHIN A STANDARD PT CRYOCOOLER

While the build-up of the full array cryocooler has been underway, we have started testing the devices within a commercial system (AC-V12 from Oxford Instruments Ltd) [15]. A single 8 x 1 pixel sub-array has been mounted to the cold finger of the cryocooler, and electrical as well as optical testing has been carried out. The main achievements of this activity have been the simultaneous operation of three bolometers, and the NETD characterization of a single pixel device. The NETD characterization was carried out by observing the photocurrent from a chopped (~100 Hz) liquid Nitrogen blackbody, and comparing the signal with the rms noise current when the LN load was blocked. The single pixel (in this measurement coupled via a 4 mm diameter Si substrate lens) demonstrated a minimum NETD of 40 mK (30 ms). This number can now be compared with the expected performance based on electrical characterization of the device: The noise current spectral density at the bottom of the I-V curve (V~5 mV) was about 10 pA/Hz$^{1/2}$, which is about a factor of six higher than expected (1.6 pA/Hz$^{1/2}$ corresponds to the intrinsic detector noise current). The electrical responsivity is simply $1/2V_0 \approx 100$ A/W, and thus the electrical NEP≈100 fW/Hz$^{1/2}$. This NEP$_e$, assuming unity coupling efficiency throughout the 4.3 THz RF bandwidth determined by the Zitex yields a unity coupling efficiency NETD of ~7 mK (30 ms). As shown in Fig. 6, the shape of the NETD –curve, as well as the clearly observable increase of pickup as the detector is biased within the superconducting transition. Both of these observations are consistent with excessive

coupling of EMI to the detector. It should also be pointed out that the experimental number for NETD is for an excessive wide bandwidth, which will be limited to ~1 THz in our future array detectors, which would correspond to a NETD of 160 mK assuming no improvements in the system optical coupling efficiency. Once the EMI issue is settled (improving noise by a factor of six), we expect to demonstrate a 0.2 to 1 THz NETD of ~30 mK. Finally, for the video rate scanning system, the per-pixel NETD will increase to 30 mK x $N_{scan}^{1/2}$=0.4 K where N_{scan} ~200 is the number of scan positions in one frame.

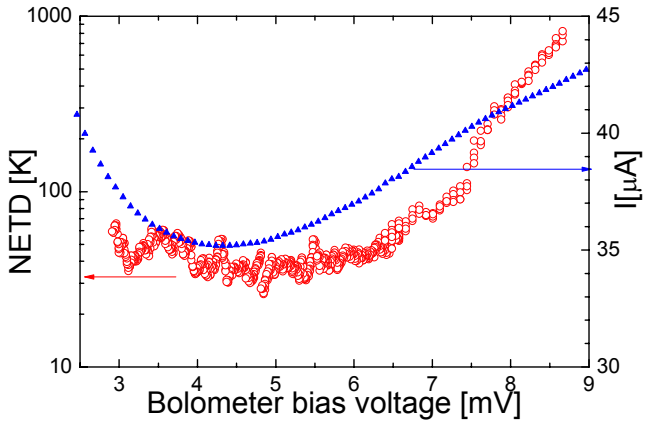

Fig. 6. The NETD of a NbN detector vs the detector bias voltage.

7. CONCLUSIONS

We have described the overall design of a ultrabroadband THz imaging system, which will be capable of video rate passive THz imaging with a per-frame thermal resolution below 0.5 K. Also, we have for the first time operated superconducting antenna-coupled microbolometer detectors within a cryogen-free refrigerator, a major step in it self towards a practical THz imaging system. Further improvements in the system performance are expected through the reduction of electrical, mechanical and thermal interference currently present in our setup.

8. ACKNOWLEDGEMENTS

The work at VTT has been party funded by TEKES the Finnish Funding Agency for Technology and Innovation, decision #40384/05. For the research carried out at NIST, the authors acknowledge the support by the Department of Homeland Security Directorate for Science and Technology, and NSF interdisciplinary award #0501578.

REFERENCES

1. C.D. Dietlein, A. Luukanen, F. Meyer, Z. Popovic, and E.N. Grossman, "*Phenomenology of Passive Broadband Terahertz Images*", presented at the 4th ESA Workshop on Millimetre-Wave Technology and Applications, Espoo, Finland (2006)
2. A. Luukanen and J.P. Pekola, "*A superconducting antenna-coupled hot-spot microbolometer*", *Appl. Phys. Lett.* vol. 82, p.3970-3972 (2003)
3. A. Luukanen, A.J. Miller and E.N. Grossman, "*Passive hyperspectral terahertz imagery for security screening using a cryogenic microbolometer*", *Proc. SPIE*, Vol. 5789, p.127-134 (2005).

4. A. Luukanen, L. Grönberg, P. Helistö, J. S. Penttilä, H. Seppä, H. Sipola, C. R. Dietlein, E. N. Grossman, " *An array of antenna-coupled superconducting microbolometers for passive indoors real-time THz imaging*", *Proc. SPIE* Vol. 6212, (2006)
5. E.N. Grossman, C.R. Dietlein, J. Chisum, and A. Luukanen, "Spectral decomposition of ultrawideband terahertz imagery", these proceedings (paper 6548-07) (2007)
6. T.-L. Hwang, S. Schwarz, and D. Rutledge, "*Microbolometers for infrared detection*," *Appl. Phys. Lett*. 34(11), pp. 773–776, 1979.
7. D.P. Neikirk, W. W. Lam, and D. B. Rutledge, "*Far-infrared microbolometer detectors*", *International journal of infrared and millimeter waves* 5(3), pp. 245–278, 1983.
8. D.P. Neikirk and D. B. Rutledge, "*Air-bridge microbolometer for far-infrared detection*", *Appl. Phys. Lett*. 44(2), pp. 153–155, 1984
9. C.R. Dietlein, A. Luukanen, J.S. Penttilä, L. Grönberg, H. Seppä, P. Helistö, and E.N. Grossman, "*Performance comparison of Nb and NbN broadband antenna-coupled microbolometers*", to be published in *SPIE* Vol. 6549 (2007)
10. A. Luukanen, E.N.Grossman, A.J. Miller, P. Helistö, J.S. Penttilä, H. Sipola, and H. Seppä, " *An Ultra-Low Noise Superconducting Antenna-Coupled Microbolometer With a Room-Temperature Read-Out*", *IEEE Microwave and Wireless Component Letters,* Vol. 16, p.464-466 (2006).
11. J. S. Penttilä, H. Sipola, P. Helistö, and H. Seppä, "*Low noise readout of superconducting bolometers based on electrothermal feedback*", *Supercond. Sci. Tech*., vol 19, no. 4, pp. 319-322, (2006)
12. http://www.cryomech.com
13. Saint-Gobain Performance Plastics, 150 Dey Road, Wayne, N.J. 07470, www.stgobain.com.
14. D. J. Benford, M. C. Gaidis, and J. W. Kooi, "*Optical Properties of Zitex in the Infrared to Submillimeter*", *Appl. Opt.* 42, p.5118-5122 (2003)
15. http:// www.oxford-instruments.com